Mononuclear (Nitrido)iron(V) and (Oxo)iron(IV) Complexes via Photolysis of [(cyclam-acetato)$Fe^{III}(N_3)$]$^+$ and Ozonolysis of [(cyclam-acetato)$Fe^{III}(O_3SCF_3)$]$^+$ in Water/Acetone Mixtures‡

Craig A. Grapperhaus,† Bernd Mienert, Eckhard Bill, Thomas Weyhermüller, and Karl Wieghardt*

Max-Planck-Institut für Strahlenchemie, Stiftstrasse 34-36, D-45470 Mülheim an der Ruhr, Germany

Received May 17, 2000

Reaction of the monoanionic, pentacoordinate ligand lithium 1,4,8,11-tetraazacyclotetradecane-1-acetate, Li(cyclam-acetate), with $FeCl_3$ yields, upon addition of KPF_6, [(cyclam-acetato)FeCl]PF_6 (**1**) as a red microcrystalline solid. Addition of excess NaN_3 prior to addition of KPF_6 yields the azide derivative [(cyclam-acetato)FeN_3]PF_6 (**2a**) as orange microcrystals. The X-ray crystal structure of the azide derivative has been determined as the tetraphenylborate salt (**2b**). Reaction of **1** with silver triflate yields [(cyclam-acetato)Fe(O_3SCF_3)]PF_6 (**3**), which partially dissociates triflate in nondried solvents to yield a mixture of triflate and aqua bound species. Each of the iron(III) derivatives is low-spin (d^5, $S = 1/2$) as determined by variable-temperature magnetic susceptibility measurements, Mössbauer and EPR spectroscopy. The low-spin iron(II) (d^6, $S = 0$) complexes $\mathbf{1_{red}}$ and $\mathbf{2a_{red}}$ have been prepared by electrochemical and chemical methods and have been characterized by Mössbauer spectroscopy. Photolysis of **2a** at 419 nm in frozen acetonitrile yields a nearly colorless species in approximately 80% conversion with an isomer shift $\delta = -0.04$ mm/s and a quadrupole splitting $\Delta E_Q = -1.67$ mm/s. A spin-Hamiltonian analysis of the magnetic Mössbauer spectra is consistent with an Fe^V ion (d^3, $S = 3/2$). The proposed [(cyclam-acetato)Fe^V=N]$^+$ results from the photooxidation of **2a** via heterolytic N−N cleavage of coordinated azide. Photolysis of **2a** in acetonitrile solution at −35 °C (300 nm) or 20 °C (Hg immersion lamp) results primarily in photoreduction via homolytic Fe−N_{azide} cleavage yielding Fe^{II} (d,[6] $S = 0$) with an isomer shift $\delta = 0.56$ mm/s and quadrupole splitting $\Delta E_Q = 0.54$ mm/s. A minor product containing high-valent iron is suggested by Mössbauer spectroscopy and is proposed to originate from [{(cyclam-acetato)Fe}$_2$(μ-N)]$^{2+}$ with a mixed-valent {Fe^{IV}(μ-N)Fe^{III}}$^{4+}$ $S = 1/2$ core. Exposure of **3** to a stream of oxygen/ozone at low temperatures (−80 °C) in acetone/water results in a single oxidized product with an isomer shift $\delta = 0.01$ mm/s and quadrupole splitting $\Delta E_Q = 1.37$ mm/s. A spin-Hamiltonian analysis of the magnetic Mössbauer yields parameters similar to those of compound II of horseradish peroxidase which are consistent with an Fe^{IV}=O monomeric complex ($S = 1$).

Introduction

Dioxygen activation by metalloenzymes and biomimetic complexes has fueled an interest in high-valent metal complexes as models for the proposed intermediates.[1−6] Formal oxidation states of +4 and +5 have been postulated for the highly oxidizing species in a number of heme and non-heme metalloproteins. For example, for cytochrome P450s it has been well established that both the metal and porphyrin ligand are redox active resulting in an (oxo)iron(IV) π-cation radical, and not an (oxo)iron(V) complex, as the catalytically relevant species.[5,7] Similar (oxo)iron(IV) π-cation radical model complexes have been obtained from (porphinato)iron(III) precursors and O-atom sources such as iodosylbenzene, *meta*-chloroperbenzoic acid (*m*CPBA), and ozone.[8−12] An analogous two electron oxidation of non-heme iron monomers with redox inactive ligands by O-atom donors would require a formal (oxo)iron(V) intermediate. However, spectroscopic evidence of such a species is lacking and for many monomeric non-heme iron enzymes the proposed activated form is a (peroxo)iron(III) species.[2,13,14] Recently, a number of (peroxo)iron(III) model complexes have been synthesized from reactions of H_2O_2 or ^{t}BuOOH and characterized by a variety of techniques including EPR, UV−vis spectroscopy, mass spectrometry, and resonance Raman spectroscopy.[15−21]

‡ Dedicated to Professor A. X. Trautwein on the occasion of his 60th birthday.

* Corresponding author. E-mail: wieghardt@mpi-muelheim.mpg.de. Phone: +49-208-306-3609. Fax: +49-208-306-3952.

† Current address: Department of Chemistry, University of Louisville, Louisville, KY 40292.

(1) See, for example: *Active Oxygen in Biochemistry*; Valentine, J. S., Foote, C. S., Greenberg, A., Liebman, J. F., Eds.; Blackie Academic & Professional: London, 1995; Vol. 3
(2) Que, L., Jr.; Ho, R. Y. N. *Chem. Rev.* **1996**, *96*, 2607−2624.
(3) Wallar, B. J.; Lipscomb, J. D. *Chem. Rev.* **1996**, *96*, 2625−2658.
(4) Kappock, T. J., Cardonna, J. P. *Chem. Rev.* **1996**, *96*, 2659−2756.
(5) Sono, M.; Roach M. P.; Coulter E. D.; Dawson J. H. *Chem. Rev.* **1996**, *96*, 2841−2887.
(6) Collins, T. J. *Acc. Chem. Res.* **1994**, *27*, 279−285.
(7) Schlichting, I.; Berendzen, J.; Chu, K.; Stock, A. M.; Maves, S. A.; Benson, D. E.; Sweet, R. M.; Ringe, D.; Petsko, G. A.; Sligar, S. G. *Science* **2000**, *287*, 1615−1622.
(8) Fujii, H.; Yoshimura, T.; Kamada, H. *Inorg. Chem.* **1997**, *36*, 6142−6143.
(9) Czarnecki, K.; Proniewicz, L. M.; Fujii, H.; Kincaid, J. R. *J. Am. Chem. Soc.* **1996**, *118*, 4680−4685.
(10) Czarnecki, K.; Nimri, S.; Gross, Z.; Proniewicz, L. M.; Kincaid, J. R. *J. Am. Chem. Soc.* **1996**, *118*, 2929−2935.
(11) Gross, Z.; Nimri, S. *Inorg. Chem.* **1994**, *33*, 1731−1732.
(12) Sugimoto, H.; Tung, H.-C.; Sawyer, D. T. *J. Am. Chem. Soc.* **1988**, *110*, 2465−2470.
(13) Feig, A. L.; Lippard, S. J. *Chem. Rev.* **1994**, *94*, 759−805.
(14) Nivorozhkin, A. L.; Girerd, J.-J. *Angew. Chem.* **1996**, *108*, 665−667; *Angew. Chem., Int. Ed. Engl.* **1996**, *35*, 609−611.

10.1021/ic0005238 CCC: $19.00
Published on Web 10/27/2000

Whereas the highly reactive (oxo)iron(V) intermediate remains elusive, Fe(V) has been spectroscopically observed with the strongly π-donating nitrido ligand. Photolysis of (azido)(porphinato)iron(III) complexes in frozen solution results in photooxidation to (nitrido)iron(V) as evidenced by the formation of a band at 876 cm^{-1} in the resonance Raman.[22] Recently we have reported the spectroscopic detection of a (nitrido)iron(V) species ($S = 3/2$) by Mössbauer and EPR spectroscopies upon the photooxidation of *trans*-[(cyclam)$Fe(N_3)_2$]ClO_4 in *frozen* acetonitrile solution.[23] The iron(V) is observable only in the immobilized matrix. The major photolysis product in *liquid* solution at room temperature is a unique nitrido-bridged dinuclear complex with *localized* antiferromagnetically coupled intermediate-spin Fe(III) ($S = 3/2$) and low-spin Fe(IV) ($S = 1$) valencies, $S = 1/2$.[23] The (μ-nitrido)diiron product results from the combination of concurrently generated (nitrido)iron(V) (via photooxidation) and iron(II) (via photoreduction) of (azido)iron(III). Although (μ-nitrido)diiron complexes ($S = 1/2$) have been previously observed upon the photolysis and/or thermolysis of phorphinato and pthalocyaninato (azido)iron(III) complexes, in those instances it was reported that the diiron core shows valence delocalization, $\{Fe^{3.5}{=}N{=}Fe^{3.5}\}^{4+}$.[24−26] In contrast to the low-spin trans isomer, photolysis of high-spin *cis*-[(cyclam)$Fe(N_3)_2$]ClO_4 in liquid solution yields a mixed valent S = 3/2 (μ-nitrido)diiron complex resulting from the antiferromagnetic coupling of high-spin Fe(III) ($S = 5/2$) and Fe(IV) ($S = 1$) localized valencies. This has also been observed for other (μ-nitrido)diiron complexes derived from high-spin non-heme (azido)iron(III) precursors.[27,28]

In this paper we describe our efforts to synthesize and spectroscopically characterize high-valent (nitrido)iron and (oxo)iron complexes in a mono-*N*-functionalized cyclam. The ligand, Li(cyclam-acetate), provides a monoanionic, pentacoordinate framework for the synthesis of a series of complexes with a single, variable coordination site. To this end, we have prepared and fully characterized monocationic iron(III) complexes of cyclam-acetate with chloride, azide, and triflate ($^{-}O_3SCF_3$) occupying the sixth coordination site. The X-ray structure of the azide derivative has been determined and is the first example of iron(III) coordinated in a mono-*N*-functionalized cyclam. Since *trans*-[(cyclam)$Fe(N_3)_2$]ClO_4 was found to yield a (μ-nitrido)diiron complex with unique magnetic properties upon photolysis in liquid solution and (nitrido)iron(V) in frozen solution, the photolysis of [(cyclam-acetato)FeN_3]PF_6 was investigated under each of these conditions. Additionally, the triflate derivative was prepared and reacted with ozone. The results of photolysis and ozonolysis are presented here.

Experimental Section

Syntheses. The ligand 1,4,8,11-tetraazacyclotetradecane-1-acetic acid tetrahydrochloride was synthesized according to published methods.[29]

^{57}Fe-enriched samples were prepared as follows. To 20 mL of concentrated HCl was added 34.55 mg of ^{57}Fe foil (98%) and 61.00 mg of natural abundance Fe metal which yielded an orange solution upon heating. Removal of solvent by rotary evaporation yielded a residue of $^{57/56}FeCl_3$ which was used in the syntheses of [(cyclam-acetato)FeX]PF_6 (X = Cl, N_3, O_3SCF_3) in reduced-scale syntheses of the procedures described below. The enrichments of ^{57}Fe (~35%) in the prepared samples were confirmed by electrospray ionization mass spectrometry.

Lithium 1,4,8,11-Tetraazacyclotetradecane-1-acetate, Li(cyclam-acetate). A 26.5 g (0.0656 mol) amount of 1,4,8,11-tetraazacyclotetradecane-1-acetic acid tetrahydrochloride was added to 100 mL of absolute ethanol. To the slurry was added 31.5 g (1.31 mol) of LiOH, and the mixture was refluxed for 24 h. The reaction mixture was then filtered and washed with 2 × 20 mL of absolute ethanol to give a yellow oily filtrate and a white solid. The volume of the filtrate was reduced by vacuum to a minimum and the oily residue stored at 4 °C for 2 days to yield a white solid. The solid was washed with 2 × 25 mL diethyl ether and dried under vacuum to yield 25.6 g of crude Li(cyclam-acetate) (48% by mass, 71% yield) which is contaminated with lithium hydroxide (see text). Further purification of the ligand was not necessary for synthesis of the following compounds. IR (KBr), ν (cm^{-1}): 2953, 2827, 1619, 1468, 1438, 1415, 1367, 1353, 1328, 1287, 1264, 1129, 1113, 1026, 834. ^{1}H NMR (D_2O), δ (ppm): 1.95 (q, 2H); 2.11 (q, 2H); 2.95 (t, 2H); 3.07 (t, 2H); 3.26 (m, 8H); 3.37 (t, 2H); 3.44 (t, 2H); 3.59 (s, 2H). ESI MS: $m/z = 257$ (m/z 257 expected for (cyclam-acetate)$^+$).

[(cyclam-acetato)$Fe^{III}Cl$]PF_6 (1). To 6.37 g (3.06 g, 11.7 mmol) of crude Li(cyclam-acetate) dissolved in 150 mL of methanol was added 1.92 g (11.9 mmol) of $FeCl_3$ in 100 mL of methanol. After 90 min of reflux, the reaction mixture was cooled to room temperature and the volume was concentrated via rotary evaporation to ~5 mL. Addition of 3.23 g (17.6 mmol) of KPF_6 as an aqueous solution (40 mL) initiated precipitation of a light red solid, which was filtered out and washed with 2 × 10 mL diethyl ether to yield 3.13 g of crude product. Pure **1** can be obtained by recrystallization from 40 mL of hot acetonitrile as a red crystalline product which was washed with diethyl ether and dried under vacuum. Yield: 1.88 g, 32%. Anal. Calcd for $C_{12}H_{25}N_4O_2FeClPF_6$: C, 29.20; H, 5.10; N, 11.35. Found: C, 29.30; H 4.98; N, 11.36. IR (KBr), $\nu_{selected}$ (cm^{-1}): 3260 (N−H), 1668 (C═O), 1299 (C−O), 839, 559 (PF_6). UV/vis recorded in MeCN (λ_{max}, ϵ (M^{-1} cm^{-1})):

(15) Bernal, I.; Jensen, I. M.; Jensen, K. B.; McKenzie, C. J.; Toftlund, H.; Tuchagues, J.-P. *J. Chem. Soc., Dalton Trans.* **1995**, 3667−3675.
(16) (a) Simaan, A. J.; Banse, F.; Mialane, P.; Boussac, A.; Un, S.; Kargar-Grisel, T.; Bouchoux, G.; Girerd, J.-J. *Eur. J. Inorg. Chem.* **1999**, 993−996. (b) Mialane, P.; Nivorojkine, A.; Pratviel, G.; Azéma, L.; Slany, M.; Godde, F.; Simaan, A.; Banse, F.; Kargar-Grisel, T.; Bouchoux, G.; Sainton, J.; Horner, O.; Guilhem; J.; Tchertanova, L.; Meunier, B.; Girerd, J.-J. *Inorg. Chem.* **1999**, *38*, 1085−1092. (c) Simaan, J.; Poussereua, S.; Blondin, G.; Girerd, J.-J.; Defaye, D.; Philouze, C.; Guilhem, J.; Tchertanov, L. *Inorg. Chim. Acta* **2000**, *299*, 221−230.
(17) Tajima, K.; Tada, K.; Jinno, J.; Edo, T.; Mano, H.; Azuma, N.; Makino, K. *Inorg. Chim. Acta* **1997**, *254*, 29−35.
(18) Guajardo, R. J.; Hudson, S. E.; Brown, S. J.; Mascharak, P. K. *J. Am. Chem. Soc.* **1993**, *115*, 7971−7977. Guajardo, R. J.; Chavez, F.; Farina, E. T.; Mascharak, P. K. *J. Am. Chem. Soc.* **1995**, *117*, 3883−3884.
(19) de Vries, M. E.; La Crois, R. M.; Roefles, G.; Kooijman, H.; Spek, A. L.; Hage, R.; Feringa, B. L. *J. Chem. Soc., Chem. Commun.* **1997**, 1549−1550.
(20) (a) Roelfes, G.; Lubben; M.; Chen, K.; Ho, R. Y. N., Meetsma, A.; Genseberger, S.; Hermant, R. M.; Hage, R.; Mandal, S. K.; Young, V. G., Jr.; Zang, Y.; Kooijman, H.; Spek, A. L.; Que, L., Jr.; Feringa, B. L. *Inorg. Chem.* **1999**, *38*, 1929−1936. (b) Zang, Y.; Kim, J.; Dong, Y.; Wilkinson, E. C.; Appleman, E. H.; Que, L., Jr. *J. Am. Chem. Soc.* **1997**, *119*, 4197−4205. (c) Roelfes, G.; Lubben, M.; Leppard, S. W.; Schudde, E. P.; Hermant, R. M.; Hage, R.; Wilkinson, E. C.; Que, L, Jr.; Feringa, B. L. *J. Mol. Catal., A* **1997**, *117*, 223−227. (d) Lubben, M.; Meetsma, A.; Wilkinson, E. C.; Feringa, B. L.; Que, L., Jr. *Angew. Chem.*, **1995**, *107*; 1610−1612; *Angew. Chem., Int. Ed.* Engl. **1995**, *34*, 1512−1514.
(21) Wada, A.; Ogo, S.; Watanabe, Y.; Mukai, M.; Kitagawa, T.; Jitsukawa, K.; Masuda, H.; Einaga, H. *Inorg. Chem.* **1999**, *38*, 3592−3593.
(22) Wagner, W.-D.; Nakamoto, K. *J. Am. Chem. Soc.* **1989**, *111*, 1590−1598.
(23) Meyer, K.; Bill, E.; Mienert, B.; Weyhermüller, T.; Wieghardt, K. *J. Am. Chem. Soc.* **1999**, *121*, 4859−4876.
(24) Bottomley, L. A.; Garrett, B. B.; *Inorg. Chem.* **1982**, *21*, 1260−1263
(25) Bottomley, L. A.; Gorce, J.-N.; Goedken, V. L.; Ercolani, C. *Inorg. Chem.* **1985**, *24*, 3733−3737.
(26) Ercolani, C.; Hewage, S.; Heucher, R.; Rossi, G. *Inorg. Chem.* **1993**, *32*, 2975−2977
(27) Jüstel, T.; Weyhermüller, T.; Wieghardt, K.; Bill, E.; Lengen, M.; Trautwein, A. X.; Hildebrandt, P. *Angew. Chem.* **1995**, *107*, 744−747; *Angew. Chem., Int. Ed. Engl.* **1995**, *34*, 669−672.
(28) Jüstel, T.; Müller; M.; Weyhermüller, T.; Kressl, C.; Bill, E.; Hildebrandt, P.; Lengen, M.; Grodzicki, M.; Trautwein, A. X.; Nuber, B.; Wieghardt, K. *Chem.−Eur. J.* **1999**, *5*, 793−810.
(29) Struder, M.; Kaden, T. A. *Helv. Chim. Acta* **1986**, *69*, 2081−2086.

228 (4500), 258 (5000), 344 (2100), 448 (55), 532 (63). ESI MS: $m/z = 348$ (m/z 348 expected for $[(\text{cyclam-acetato})Fe^{III}Cl]^+$.

[(cyclam-acetato)FeN$_3$]X (X = PF$_6$ (2a), BPh$_4$ (2b)). To 1.83 g (0.878 g, 3.36 mmol) of crude Li(cyclam-acetate) dissolved in 40 mL of H_2O was added 0.570 g (3.52 mmol) of $FeCl_3$ dissolved in 40 mL of H_2O. The resulting solution was brought to a gentle reflux and heating continued for 60 min as a dark red color developed. The solution was cooled to room temperature, and an excess, 0.720 g (11.1 mmol), of NaN_3 was added. The resulting solution was stirred for 2 h at room temperature and subsequently filtered to yield a clear red filtrate. Addition of 2.00 g (10.9 mmol) of KPF_6 as an aqueous solution (40 mL of H_2O) yielded red-orange microcrystals of **2a** upon cooling at 4 °C overnight, which were collected by filtration, washed with 2 × 25 mL diethyl ether, and dried under vacuum. Yield: 1.00 g, 60%. Anal. Calcd for $C_{12}H_{25}N_7O_2FePF_6$: C, 28.82; H, 5.04; N, 19.60. Found: C, 29.37; H 5.07; N, 19.24. IR (KBr), $\nu_{selected}$ (cm^{-1}): 3261 (N−H), 2051 (N_3), 1664 (C═O), 1285 (C−O), 836, 559 (PF_6). UV/vis recorded in MeCN (λ_{max}, ϵ (M^{-1} cm^{-1})): 245 (11 100), 277 (sh), 306 (4570), 458 (2550). ESI MS: $m/z = 355$ (m/z 355 expected for $[(\text{cyclam-acetato})Fe^{III}N_3]^+$.

Addition of excess $NaBPh_4$ in a 1:1 mixture of H_2O−acetonitrile to 100 mg of **2a** dissolved in 10 mL of acetonitrile yielded orange needle shaped crystals of **2b** suitable for X-ray crystallography upon slow evaporation of solvent. Anal. Calcd for $C_{36}H_{45}N_7O_2FeB$: C, 64.11; H, 6.73; N, 14.54. Found: C, 64.22; H 6.64; N, 14.63. ESI MS: $m/z = 355$ (m/z 355 expected for $[(\text{cyclam-acetato})Fe^{III}N_3]^+$.

[(cyclam-acetato)Fe(O$_3$SCF$_3$)]PF$_6$ (3). To 0.984 g (1.99 mmol) of **1** dissolved in 50 mL of dry acetonitrile was added a slight excess, 0.680 g (2.65 mmol), of silver triflate. The reaction was brought to gentle reflux and heating continued for 60 min as a white precipitate developed. The reaction mixture was cooled to room temperature and then anaerobically filtered through a bed of Celite to remove solid AgCl. The volume of the red-orange filtrate was reduced under vacuum to ~2 mL followed by addition of 15 mL of diethyl ether to yield **3** as a hygroscopic pale pink powder. The ether was carefully decanted and the solid dried under vacuum. Yield: 1.04 g, 86%. Anal. Calcd for $C_{13}H_{25}N_4O_5SPF_9Fe$: C, 25.71; H, 4.15; N, 9.23. Found: C, 25.55; H 4.13; N, 9.30. IR (KBr), $\nu_{selected}$ (cm^{-1}): 3271 (N−H), 1666 (C═O), 1279 (C−O), 1256 (SO_2), 1178 (C−F), 1033 (SO_2), 843 (PF_6), 639, 559 (PF_6). ESI MS: $m/z = 462$, 330 (m/z 462 expected for $[(\text{cyclam-acetato})Fe^{III}(O_3SCF_3)]^+$, m/z 330 expected for m/z 462 − triflate + H_2O).

Physical Measurements. Infrared spectra (400−4000 cm^{-1}) as KBr disks or as acetonitrile solutions were performed on a Perkin-Elmer 2000 FT-IR/FT-NIR spectrometer with a resolution of 4 cm^{-1}. UV−visible measurements were performed with a Hewlett-Packard 8452A diode array spectrophotometer for photolysis and coulometric experiments and either the HP 8452A or a J&M (Aalen, Germany) Tidas array detector (200−620 and 600−1010 nm) using a J&M LDH light source for ozonolysis experiments. Cyclic voltammograms and coulometric measurements were recorded as acetonitrile solutions with 0.1 M tetra-*n*-butylammonium hexafluorophosphate as supporting electrolyte using an EG & G potentiostat/galvanostat (model 273A) and are referenced versus ferrocenium/ferrocene. Elemental analysis were performed by H. Kolbe Mikroanalysis in Mülheim an der Ruhr, Germany. ^1H and ^{13}C NMR measurements were recorded in deuterated solvents on a 400 MHz Bruker AMX series spectrometer. Electrospray ionization mass spectra were determined using a Finnigan MAT 95 spectrometer, Finnigan GmbH, Bremen, Germany.

X-band EPR spectra were determined with a Bruker ESP 300E spectrometer equipped with a helium flow cryostat (Oxford Instruments ESR 910). Mössbauer data were recorded on an alternating constant-acceleration spectrometer. The minimum experimental line width was 0.24 mm s^{-1} (full width at half-height). A constant sample temperature was maintained with an Oxford Instruments Variox or an Oxford Instruments Mössbauer-Spectromag 2000 Cryostat. The latter is a split-pair superconducting magnet system for applied fields up to 8 T in which the sample temperature can be varied between 1.5 and 250 K with the field of the sample oriented perpendicular to the γ-beam. The $^{57}Co/Rh$ source (1.8 GBq) was positioned at room temperature inside the gap of the magnet system at a zero-field positions. Reported isomer shifts (δ) are referenced versus iron metal at 300 K. Low-temperature magnetic Mössbauer spectra were analyzed on the basis of a spin-Hamiltonian description of the electronic ground-state spin multiplet

$$H_e = D[S_z^2 - S(S+1)/3 + (E/D)(S_x^2 - S_y^2)] + \mu_B \mathbf{B}\cdot\bar{\mathbf{g}}\cdot\mathbf{S} \quad (1)$$

with $S = 3/2$, $S = 1$, or $S = 1/2$ being the spin of the corresponding system. The parameters D and E/D are the axial and rhombic zero-field parameters for $S = 3/2$, $S = 1$, or $S = 1/2$. The hyperfine coupling was calculated by using the additional term

$$H_{hf} = \langle \mathbf{S} \rangle \bar{\mathbf{A}}\cdot\mathbf{I} - g_N\beta_N\mathbf{B}\cdot\mathbf{I} + H_Q \quad (2)$$

where $\langle \mathbf{S} \rangle$ is the electronic spin expectation value, $\bar{\mathbf{A}}$ is the hyperfine coupling tensor, $\mathbf{I}$ is the nuclear spin, and H_Q is the usual nuclear quadrupole Hamiltonian.[30] Simulations of the frozen solution EPR spectra were performed with a program for spin = 1/2 and effective g values.

X-ray Crystallography. An orange crystal of **2b** was mounted in a sealed in glass capillary. Graphite-monochromated Mo Kα radiation ($\lambda = 0.710\ 73$ Å) was used. Crystallographic data are listed in Table 1. Intensity data were collected at 100(2) K on a Siemens SMART CCD-detector system equipped with a cryogenic nitrogen cold stream. The data were corrected for Lorentz and polarization effects. A semiempirical absorption correction was made using the SADABS[31] program. The solution, refinements, and graphical representation of the structure were performed using the Siemens ShelXTL[32] software package. The structure was solved and refined by direct methods and difference Fourier techniques. Neutral atom scattering factors were used.[33] All hydrogen atoms were placed at calculated positions and refined as riding atoms with isotropic displacement parameters. All non-hydrogen atoms were refined anisotropically.

Photolysis Experiments. Photolyses of solutions of **2a** in dry, deaerated acetonitrile were performed at 20 and −35 °C in variable-temperature quartz cells. A stream of argon was purged through the solution during irradiation with a Hg immersion lamp (Osram, HPK 125) or via a Rayonet Photochemical Reactor (RPR-100) equipped with 300 nm tubes. During photolysis sample portions were removed via

Table 1. Crystallographic Data for 2b·MeCN

chem formula	$C_{38}H_{48}BFeN_8O_2$
fw	715.50
space group	$P2_1/n$
a, Å	11.945(2)
b, Å	12.599(2)
c, Å	24.455(4)
α, deg	90
β, deg	102.20(2)
γ, deg	90
V, Å	3597(1)
Z	4
T, K	100
radiation λ, Å	0.71073
ρ_{calcd}, g cm^{-3}	1.321
μ(Mo Kα), cm^{-1}	4.65
reflcns collcd	33 835
unique reflcns/obsd [$I > 2\sigma(I)$]	10 115/6926
no. of params	452
R1[a] [$I > 2\sigma(I)$]	0.0465
wR2[b] [$I > 2\sigma(I)$]	0.0976

[a] $R1 = \Sigma||F_o| - |F_c||/\Sigma|F_o|$, $R_W = [\Sigma w(|F_o| - |F_c|)^2/\Sigma w F_o^2]^{1/2}$, where $w = 4F_o^2/\sigma^2(F_o^2)$. [b] $wR2 = [\Sigma[w(F_o^2 - F_c^2)^2]/\Sigma[w(F_o^2)]^2]^{1/2}$, where $w = 1/\sigma^2(F_o^2) + (aP)^2 + bP$, $P = (F_o^2 + 2F_c^2)/3$.

(30) Gütlich, P.; Link, R.; Trautwein, A. *Mössbauer Spectroscopy and Transition Metal Chemistry*; Springer-Verlag: Berlin, Heidelberg, New York, 1978.
(31) Sheldrick, G. University of Göttingen, 1994.
(32) *ShelXTL V.5*; Siemens Analytical X-ray Instruments, Inc.: Madison, WI, 1994.
(33) *International Tables for X-ray Crystallography*; Kynoch Press: Birmingham, England.

syringe for analysis (UV−vis, EPR, and IR). Samples for photolysis in frozen acetonitrile were prepared as previously reported for *trans*-[(cyclam)Fe(N_3)$_2$]ClO_4 with samples photolyzed via method II[23] for 90 min.

Ozonolysis Experiments. In a typical experiment, 18 mg (0.030 mmol) of **3** was dissolved in 2 mL (15 mM) of acetone/water (95:5 v/v) in a small test tube. If necessary, the solution was filtered to remove trace amounts of silver impurities. The test tube was placed in a precooled brass block (−80 °C) located in a dewar. The temperature of the block was monitored during the reaction and remained constant within ±5 °C. A stream of ozone provided by an ozone generator (SWO-70 Wedeco, Herford, Germany) was passed through the solution for up to 30 min. Within 1 min the pink color of **3** initially fades and then darkens to green. For collection of samples for Mössbauer spectroscopy, ozonolysis was performed in a 3 cm glass tube with a Teflon Mössbauer sample holder affixed to one end. The sample was immediately frozen in liquid nitrogen following ozonolysis. For UV−visible measurements *during* ozonolysis, the reaction was performed in quartz UV−vis cell at −40 °C with suspension of the ozone/oxygen stream during measurements.

Results and Discussion

Syntheses and Characterization. The coordination of first row transition metals in monofunctionalized cyclam derivatives has largely focused on complexes of nickel(II), copper(II), and cobalt(II).[34] Prior to this current report, no monofunctionalized cyclam complexes have been reported for iron although the C-functionalized dicarboxylato- and diaminocyclam complexes are known.[35,36]

Utilizing the mono-*N*-functionalized derivative of cyclam 1,4,8,11-tetraazacyclotetradecane-1-acetic acid, H(cyclam-acetate), previously reported by Struder and Kaden,[29] a series of complexes with the general formula [(cyclam-acetato)FeX]Y has been prepared. The new complexes and labeling scheme are summarized in Scheme 1. Coordination of H(cyclam-acetate) to iron requires deprotonation of the ligand in ethanol with a large excess of lithium hydroxide prior to the addition of iron(III) chloride. Although the crude ligand contains significant quantities of lithium hydroxide, approximately 52% by mass as determined by elemental analysis, further purification is not required for the syntheses of the complexes presented below in reasonable yields (32−60%). In fact, no iron complexation occurs if the pH of the ligand solution is adjusted to 7 prior to the addition of iron(III) chloride or if H(cyclam-acetate) is employed as the ligand source.

Scheme 1 depicts the synthetic methods for the preparation of **1**−**3**. Iron(III) chloride reacts with Li(cyclam-acetate) in refluxing methanol to yield, upon addition of KPF_6, [(cyclam-acetato)$Fe^{III}Cl$]PF_6 (**1**) as a crude, red powder. Recrystallization from hot acetonitrile yields **1** as a dark red, crystalline solid. The azide derivative, [(cyclam-acetato)$Fe^{III}N_3$]PF_6 (**2a**), can be obtained by reaction of **1** with excess NaN_3, although better overall yields are obtained via a one-pot synthesis. Following the reaction of $FeCl_3$ and Li(cyclam-acetate) in aqueous solution, addition of an excess of NaN_3 followed by the addition of KPF_6 initiates precipitation of **2a** as orange microcrystals upon cooling at 4 °C overnight. Exchange of hexafluorophosphate for tetraphenylborate yields, upon slow evaporation of solvent, crystals of [(cyclam-acetato)$Fe^{III}N_3$]BPh_4 (**2b**) suitable for X-ray crystallographic analysis. Addition of silver triflate to a dry acetonitrile solution of **1** results in the exchange of the coordinated chloride with triflate yielding [(cyclam-acetato)-$Fe^{III}O_3SCF_3$]PF_6 (**3**) as a light pink, hygroscopic powder.

Scheme 1

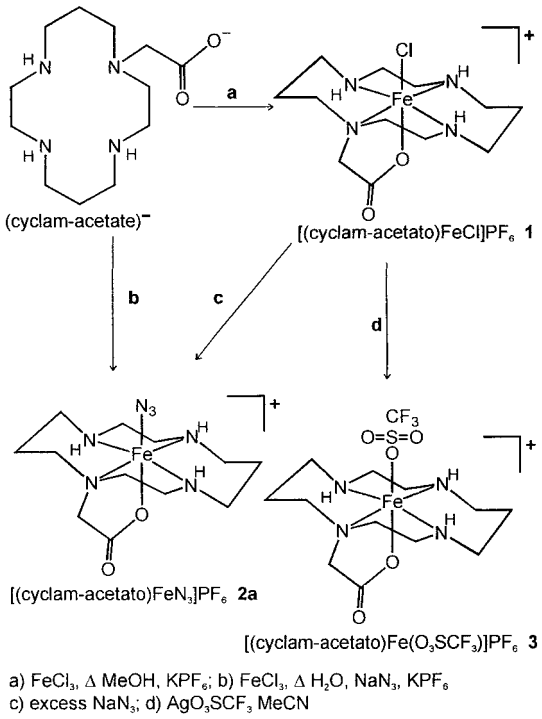

The infrared spectra of the iron complexes **1**−**3** each display bands which are assigned to the asymmetric and symmetric stretching modes of the carboxylate functionality in the range of 1664−1668 and 1275−1299 cm^{-1} consistent with monodentate coordination of the carboxylate. The azide bound derivative **2a** displays an intense $\nu_{as}(N_3)$ vibration at 2051 cm^{-1} comparable to that observed at 2044 cm^{-1} for *trans*-[(cyclam)-Fe(N_3)$_2$]ClO_4.[23] From temperature-dependent magnetic susceptibility measurements, the magnetic moments of **1** and **2b** measured at 298 K are 2.13 and 2.14 μ_B, respectively. The magnetic susceptibility of **1** and **2b** display a temperature dependence (2−300 K) that can be satisfactorily fit with $S = 1/2$, $g = 2.220$, and a temperature-independent paramagnetism (TIP) of 3.35×10^{-4} cm^3/mol for **1** and with $S = 1/2$, $g = 2.245$, and a TIP of 1.15×10^{-4} cm^3/mol for **2b**. These results are consistent with iron(III) in the low-spin configuration. The magnetic susceptibility of **3** is also consistent with low-spin Fe(III) with *g*-values determined by EPR (vide infra). For iron(III) complexes of the general formula [(cyclam)Fe(X)$_2$]$^+$, the planar N_4 arrangement of the trans conformation is exclusively observed for the smaller, low-spin ion (0.69 Å) whereas the larger high-spin iron(III) ion (0.785 Å) requires the cyclam to adopt a cis orientation.[23,37] Thus, the spin state of complexes **1**−**3** is consistent with a relatively planar N_4 coordination with axial coordination of the acetate oxygen and chloride, azide, or triflate for **1**−**3**, respectively.

The X-band EPR spectrum of **1**, Figure S1 (top), displays a rhombic signal consistent with the assignment of low-spin iron(III) ($S = 1/2$). The spectrum can be satisfactorily simulated with $g_1 = 2.90$, $g_2 = 2.29$, and $g_3 = 1.78$. Analysis of the *g*-values using the ligand-field model developed by Griffith[38]

(34) Bernhardt, P. V.; Lawrance, G. A. *Coord. Chem. Rev.* **1990**, *104*, 297−343.
(35) Curtis, N. F.; Xin, L.; Weatherburn, D. C. *Inorg. Chem.* **1993**, *32*, 5838−5843.
(36) (a) Bernhardt, P. V.; Hambley, T.; Lawrance, G. A. *J. Chem. Soc., Chem. Commun.* **1989**, 553−554. (b) Bernhardt, P. V.; Comba, P.; Hambley, T. W.; Lawrance, G. A. *Inorg. Chem.* **1991**, *30*, 942−946.
(37) Chan, P.-K.; Poon, C.-K. *J. Chem. Soc., Dalton Trans.* **1976**, 858−862.

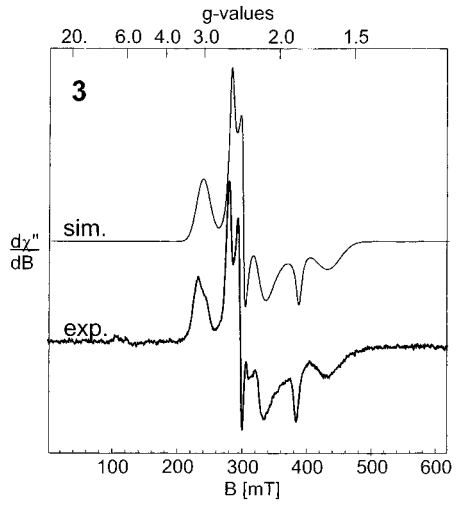

Figure 1. X-band EPR spectrum of **3** in frozen acetonitrile at 10 K. Experimental conditions: microwave frequency 9.64 GHz; microwave power 100 μW; modulation amplitude 1.1 mT. The simulation is powder calculations performed with effective g-values and consists of two overlapping subspectra (3:7) (Kramer's doublets of $S = 1/2$): $\bar{g}_A =$ (2.50, 2.35, 1.83), anisotropic line widths $\bar{W}_A =$ (10.9, 8.9, 12.5) mT (Lorentzian); $\bar{g}_B =$ (2.96, 2.19, 1.63), anisotropic line widths $\bar{W} =$ (26.8, 30.6, 48.9) mT (Lorentzian).

and extended by Taylor[39] for the spin−orbit interaction of low-spin iron(III) porphyrin complexes indicates that the unpaired electron is almost exclusively (~97%) in the *xz* or *yz* orbital consistent with a $(d_{xy})^2(d_{xz}, d_{yz})^3$ ground state as expected for a compressed octahedron. The resulting energy splitting of the t_{2g} orbitals consists of a strong tetragonal contribution $\Delta/\lambda =$ 4.84 and a large rhombic component $|V/\lambda| = 2.39$, where λ is the spin−orbit coupling constant, inset Figure S1 (top).

Solutions of complex **2a** in acetonitrile show only broad EPR spectra at X-band frequencies without resolved lines, even in diluted samples. Although the concentration affects the shape of the spectra and the total width of the resonances, resolved principal g values can only be determined if higher frequencies are used. Measurements at Q-band yield partially resolved rhombic spectra from which the values $g_1 = 1.914$, $g_2 = 2.264$, and $g_3 = 2.545$ were determined (Figure S1, bottom) consistent with $S = 1/2$, low-spin iron(III). We assume that intermolecular spin interaction, which is less important at the higher resonance fields at Q-band, is the origin of the frequency dependence. A g-value analysis within the ligand field model for a "proper" axes system ($V/\Delta < 2/3$) indicates a $(d_{xz}, d_{yz})^4(d_{xy})^1$ ground state, with strong tetragonal orbital splitting, $|\Delta/\lambda = 5.7|$, and a large rhombic component $|\Delta/\lambda| = 3.9$ ($V/\Delta = 0.63$).

The EPR spectrum of **3** recorded in frozen acetonitrile displays two overlapping rhombic signals, Figure 1. The spectrum is satisfactorily simulated with $g_1 = 2.50$, $g_2 = 2.35$, and $g_3 = 1.83$ for the narrower, less intense (45% relative intensity) subspectrum a and $g_1 = 2.96$, $g_2 = 2.19$, and $g_3 = 1.63$ for the broader, more intense (55% relative intensity) component (subspectrum b). The broad signal is assigned to the aqua species $[(\text{cyclam-acetato})\text{Fe}(\text{OH}_2)]^{2+}$ resulting from the displacement of the triflate ion by trace water upon dissolution and not from an impurity in the sample. The Mössbauer spectrum of a powder sample of **3** displays a single quadrupole doublet whereas dissolution complicates the spectrum (vide infra). Elemental analysis of **3** is consistent with the proposed formulation for the triflate-bound species $C_{13}H_{25}N_4O_5FePF_9S$ (see Experimental Section). Electrospray ionization mass spectroscopy reveals the expected ion for $[(\text{cyclam-acetato})\text{Fe}^{\text{III}}(O_3SCF_3)]^+$ at $m/z = 462$ and a second ion at $m/z = 330$ consistent with the loss of triflate and coordination of water.

Table 2. Mössbauer Data for Iron(III) and Iron(II) Complexes[a]

	complex	T (K)	δ (mm/s)	ΔE_Q (mm/s)	Γ (mm/s)
1	powder	80	0.28	2.66	0.42
2a	CH_3CN	80	0.27	2.53	0.64
3	powder	80	0.26	2.82	0.95
$\mathbf{1}_{red}$	CH_3CN	80	0.56	0.52	0.27
$\mathbf{2}_{red}$	CH_3CN	80	0.56	0.54	0.46

[a] Estimated errors of ±0.02 in δ, ±0.04 in ΔE_Q, and ±0.02 in Γ.

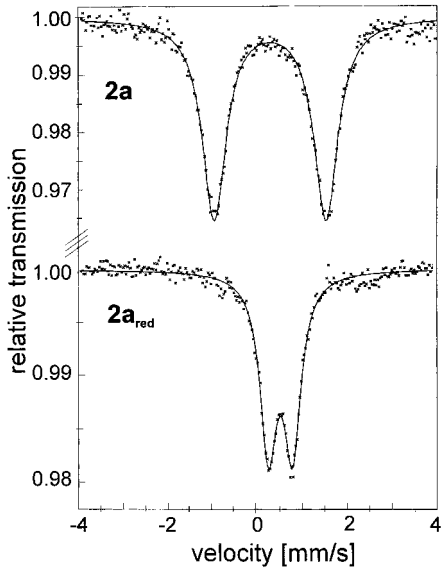

Figure 2. Zero-field Mössbauer spectra of **2a** (80 K, 20 mM acetonitrile, top) and the chemically reduced $\mathbf{2a}_{red}$ (80 K, 20 mM acetonitrile, bottom). The solid lines result from a spin-Hamiltonian simulation as described in the text.

The zero-field Mössbauer spectra of **1** and **2a** recorded at 80K each display a single quadrupole doublet with parameters summarized in Table 2. The spectrum of **1** recorded as a powder displays an isomer shift, δ, of 0.28 mm/s, a quadrupole splitting, ΔE_Q, of 2.66 mm/s, and a line width, Γ, of 0.42 mm/s. Complex **2a**, in frozen acetonitrile, displays a similar Mössbauer spectrum, Figure 2, with $\delta = 0.27$ mm/s, $\Delta E_Q = 2.49$ mm/s, and $\Gamma =$ 0.64 mm/s. The isomer shift values for **1** and **2a** are in the range expected for low-spin (cyclam)Fe(III) complexes and the large quadrupole splitting supports a nonspherical electron distribution, t_{2g}^5, confirming the low-spin assignment made from magnetic susceptibility and EPR measurements.[23]

A zero-field Mössbauer spectrum of **3** (80 K) recorded as dry powder is shown in Figure 3 and consists of a single, quadrupole doublet. The values for the isomer shift, $\delta = 0.26$ mm/s, and quadrupole splitting, $\Delta E_Q = 2.82$ mm/s, are similar to those observed for **1** and **2a**. Complex **3** was also measured in frozen acetone/water mixture (95:5, 35% ^{57}Fe-enriched) in order to obtain reference spectra of the starting samples for the ozonolysis described below. However, since intermediate spin relaxation in the 80 K spectra leads to inhomogeneous superpositions of magnetically broadened components, we refrained from further analysis of these spectra (for details see below, Figure S3).

Magnetic Mössbauer spectra of **2a** and **3** in solution were measured at 2 and 160 K with fields of 2−7 T applied

(38) Griffith, J. S. *Proc. R. Soc. London, A* **1956**, *235*, 23−36.
(39) Taylor, C. P. S. *Biochim. Biophys. Acta* **1997**, *491*, 137−149.

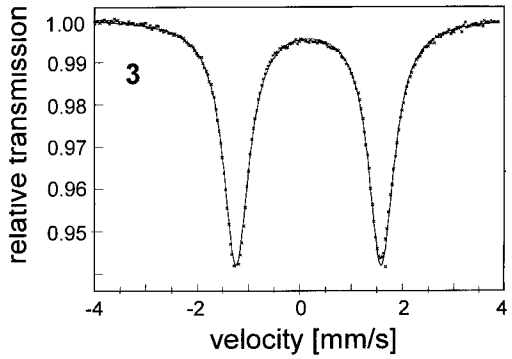

Figure 3. Zero-field Mössbauer spectrum of **3** (80 K, powder). The solid line results from a spin-Hamiltonian simulation as described in the text.

Table 3. Spin-Hamiltonian and Hyperfine Parameters of the Low-spin (t_{2g}^5, $S = 1/2$), Iron(III) Complexes **2a** and **3**

	2a	**3**
δ, mm/s	0.27	0.27
ΔE_Q, mm/s[d]	−2.53	−2.94
$\bar{g}$	1.914, 2.264, 2.545[a]	1.63, 2.19, 2.96[b]
$\bar{A}/g_N\beta_N$, T	−41.17, 34.98, −6.32	−43.40, 48.82, 9.79
η	0.40	0.41
Euler angles (α, β, γ), deg	12, −144, 0	0, −111, 0

[a] Taken from Q-band EPR measurements. [b] Taken from X-band EPR measurements.

perpendicular to the γ-rays. Resolved hyperfine pattern with wide and asymmetric line splittings were obtained (Figures S2 and S3) similar to what was found for the low-spin *trans*-[(cyclam)Fe$(N_3)_2]^+$.[23] The spectra could be reasonably well fitted by spin-Hamiltonian simulations based on EPR *g*-values taken from EPR spectra of the same solutions. The obtained simulation parameters are given in Table 3. The expected inhomogeneity resulting from the two slightly different iron(III) low-spin species found in the EPR spectrum of **3** (40:60 superposition) could not be resolved in the corresponding Mössbauer spectrum. For both compounds, **2a** and **3** (average spectra), the negative sign of V_{zz}, the moderately strong asymmetry parameters $\eta \approx 0.4$, and the orientation of the efg and anisotropic $\bar{A}$-tensor components are consistent with the ligand field description of the iron(III) low-spin $(t_{2g})^5$ configuration as it was derived from the EPR *g*-values.

The molecular structure of **2b** consists of a [(cyclam-acetato)-$FeN_3]^+$ cation, one acetonitrile molecule of crystallization, and a single, uncoordinated tetraphenylborate anion as determined by X-ray crystallography. Each cation is linked to two other cationic units via a hydrogen-bonding network between O(2) and N(4) (N···O 2.861 Å). Additionally, a hydrogen bond is proposed between the cyclam amine N(4) and N(8) of the acetonitrile molecule (N···N 2.983 Å). A summary of the X-ray experimental conditions and data collections is provided in Table 1.

A representation of [(cyclam-acetato)$FeN_3]^+$ is shown in Figure 4 with selected bond distances and angles listed in Table 4. The iron of **2b** sits in a compressed octahedral environment with the four cyclam nitrogens occupying the equatorial positions and the carboxylate oxygen filling one of the axial sites with the azide ligand occupying the site trans to the carboxylate. The cyclam adopts the most favored trans III configuration as defined by Bosnich et al.[40] The complex exhibits typical Fe−N distances to the secondary amines N(2), N(3), and N(4) of 2.001(2), 2.007(2), and 2.002(1) Å for low-

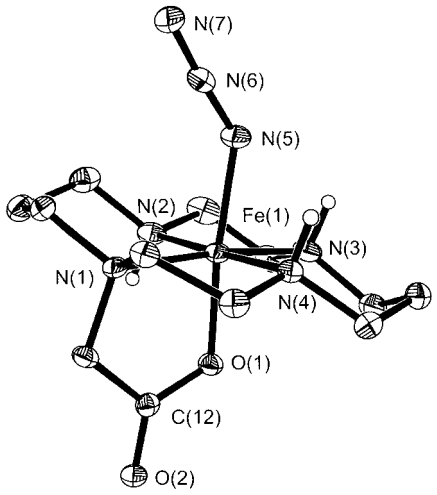

Figure 4. View of the molecular structure and atom labeling of the monocation in crystals of **2b**. Small open circles represent amine hydrogen atoms. Other hydrogen atoms have been eliminated.

Table 4. Selected Bond Lengths (Å) and Angles (deg) for **2b**

Fe−N1	2.028(2)	N1−Fe−N2	92.83(6)
Fe−N2	2.001(2)	N2−Fe−N3	85.97(7)
Fe−N3	2.007(2)	N3−Fe−N4	95.59(6)
Fe−N4	2.002(2)	N4−Fe−N1	86.78(6)
Fe−N5	1.931(2)	N1−Fe−N3	173.94(6)
Fe−O1	1.889(1)	N2−Fe−N4	178.29(6)
C12−O1	1.303(2)	O1−Fe−N5	172.74(6)
C12−O2	1.221(2)	Fe−N5−N6	131.8(1)
N5−N6	1.209(2)	N5−N6−N7	175.7(2)
N6−N7	1.156(2)		

spin Fe(III) cyclam complexes.[23] The Fe−N(1) bond distance to the tertiary amine is slightly longer, 2.028(2) Å. The 4 nitrogens of the macrocycle form a distorted plane with a mean deviation of 0.066 Å. The $Fe-N_{azide}$ distance 1.931(2) Å is essentially the same as that reported for *trans*-[(cyclam)Fe-$(N_3)_2]^+$, 1.937(2) Å.[23] The rather short $Fe-O_{acetate}$ bond distance of 1.889(1) Å is similar to that reported for a carbon-substituted dicarboxylic acid derivative of cyclam which has an average Fe−O bond distance of 1.895(2) Å.[35]

On the basis of the structural determination by X-ray crystallographic methods of **2b** and the similarities in the spectroscopy of **1**−**3**, it is proposed that the iron in each of the complexes is coordinated in a similar environment, that is, nearly planar coordination of the four nitrogen donor of cyclam with axial coordination of the tethered carboxylate functionality. The sixth coordination site is occupied by chloride, azide, or triflate/water for **1**, **2a,b**, and **3,** respectively.

Electrochemical Investigations. The electrochemistry of **1** and **2a** was investigated in acetonitrile solution with 0.1 M [(*n*-$Bu)_4N]PF_6$ (TBAHFP) as supporting electrolyte by cyclic voltammetry. All potentials reported are referenced versus the ferrocenium/ferrocene couple (0.40 V versus NHE). A summary of observed electrochemical potentials is provided in Table 5.

The cyclic voltammogram of **1**, measured at a scan rate of 200 mV/s, displays a reversible reduction wave, Fe(III)/Fe(II), at −640 mV, Figure S4. Absorbance spectra recorded in situ during coulometry (−1.1 V) display isosbestic points at 316 and 374 nm upon the one electron reduction of **1**, Figure S5. Following reduction, the sample was monitored for 30 min via square wave voltammetry during which time a slow decay of

(40) (a) Bosnich, B.; Poon, C.-K.; Tobe, M. L. *Inorg. Chem.* **1965**, *4*, 1102−1108. (b) Adam, K. R.; Atkinson, I. M.; Lindoy, L. F. *Inorg. Chem.* **1997**, *36*, 480−481.

Table 5. Electrochemical Data[a] from Cyclic Voltammetry in Acetonitrile[b] of **1** and **2a**

complex	$E_{1/2}$ (ΔE_p) (mV)	i_{pa}/i_{pc}	assgnt
1	−640 (100)	0.87	Fe(III)/Fe(II)
	+1300 (irr)[c]		
2a	−750 (83)	0.86	Fe(III)/Fe(II)
	+990 (86)[d]	1.06[d]	

[a] All potentials are measured at a scan rate of 200 mV/s unless otherwise noted and are referenced to ferrocenium/ferrocene standard. [b] ~1 mM solution with 0.1 M TBAHFP supporting electrolyte measured versus $Ag/AgNO_3$ reference electrode. [c] The process is irreversible. The potential reported is the E_{pc} measured at 200 mV/s. [d] Measured at a scan rate of 20 V/s.

the original signal was observed but no new signals were detected. This is in contrast to the observed isomerization of *trans*-$[(cyclam)Fe(N_3)_2]^+$ to the cis isomer upon reduction of the iron from +3 to +2 oxidation state.[23] The lack of isomerization for the substituted cyclam complex is attributed to ligation of the pendant carboxylate functionality which apparently favors the trans cyclam orientation even with the larger ionic radius of Fe(II). Chemically reduced samples of **1** prepared by addition of 1 equiv of lithium triethylborohydride (Super-Hydride) to a solution which were frozen for Mössbauer analysis display a single quadrupole doublet with $\delta = 0.56$ mm/s and $\Delta E_Q = 0.52$ mm/s, Table 2. The +0.30 mm/s shift in the isomer shift is consistent with a change in the formal of oxidation state from +3 to +2. Also, the small quadrupole splitting indicates a spherical distribution of electron density consistent with a retention of the low-spin state, t_{2g}^6. Upon exposure to air, $\mathbf{1_{red}}$ quickly degrades yielding an orange precipitate of uncharacterized iron products and free ligand. Complex **1** also displays an oxidation at 1330 mV which is irreversible at a scan rate of 200 mV/s.

Complex **2a** displays electrochemistry which is similar to that of **1**. The cyclic voltammogram, Figure S6, measured at 200 mV/s shows a reversible reduction at −750 mV and a quasi-reversible oxidation at +990 mV. The oxidation becomes reversible at fast scan rates (above 800 mV/s). The reduction potential is essentially the same as that observed for *trans*-$[(cyclam)Fe(N_3)_2]^+$ (−760 mV) and is assigned to an Fe(III)/Fe(II) redox couple. Upon bulk reduction of **2a**, a decrease in the absorbance spectrum at 458 nm and at 302 nm is observed. As with $\mathbf{1_{red}}$, there is no evidence that $\mathbf{2_{red}}$ isomerizes to the cis conformation. The Mössbauer spectrum of chemically generated $\mathbf{2_{red}}$ displays a single quadrupole doublet with $\delta = 0.56$ mm/s and $\Delta E_Q = 0.54$ mm/s (Table 2) consistent with low-spin Fe(II), Figure 2 (bottom).

Photolysis of 2a in Liquid Acetonitrile. Photolysis of a 20 mM solution **2a** in dry, deaerated acetonitrile was performed at ambient temperature with a medium-pressure mercury lamp. The solution was purged with Ar during photolysis, and aliquots were removed every 5 min for analysis by IR spectroscopy (2150−1900 cm^{-1}). Within the first 5 min a significant decrease in the intensity of the $\nu_{as}(N_3)$ (2051 cm^{-1}) occurs with nearly complete attenuation after 30 min. The intensity loss in the IR spectrum is accompanied by a color change from orange to brown/green. Since prolonged photolysis results in further degradation of the complex (vida infra), a sample was removed after 10 min photolysis (~2/3 completion as determined by IR) and frozen for Mössbauer analysis.

The most striking feature in the zero-field Mössbauer spectrum (80 K) of photolyzed **2a**, Figure 5, is the intense quadrupole doublet, subspectrum b, with $\delta = 0.56$ mm/s and $\Delta E_Q = 0.54$ mm/s which accounts for 52% of the spectral

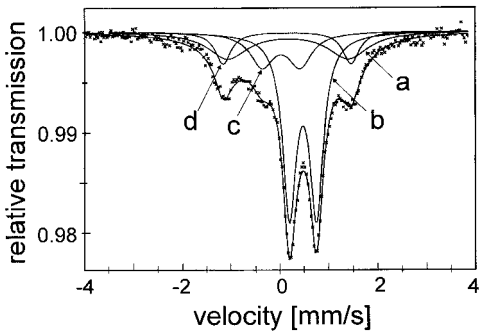

Figure 5. Zero-field Mössbauer spectrum of **2a** in CH_3CN (20 mM) after 10 min of irradiation with a Hg-immersion lamp at room temperature. The fit was obtained with four subspectra: starting material **2a** (a); low-spin Fe(II) (b); low-spin Fe(IV) (c); low-spin Fe(III) (d). See text for δ and ΔE_Q parameters.

intensity. Subspectrum b displays isomer shift and quadrupole splitting parameters identical to those of $\mathbf{2_{red}}$ and is assigned to a low-spin Fe(II) complex. Unreacted **2a** is also present at 21% relative intensity, subspectrum a. The remaining 27% of the intensity was fit with parameters similar to those of the $\{Fe^{IV}(\mu\text{-}N)Fe^{III}\}$ dimer obtained upon photolysis of *trans*-$[(cyclam)Fe(N_3)_2]ClO_4$:[23] (c) $\delta = 0.12$ mm/s, $\Delta E_Q = 0.80$ (16% relative intensity); (d) $\delta = 0.25$ mm/s, $\Delta E_Q = 2.64$ mm/s (11% relative intensity). Prolonged photolysis is accompanied by the appearance of a new, uncharacterized subspectrum with $\delta = 0.42$ mm/s, $\Delta E_Q = 1.20$ mm/s.

Photolysis of **2a** was also performed at 300 nm at low temperature (−35 °C) in an attempt to promote the formation/stability of high-valent Fe and hence the relative yield of the $\{Fe^{IV}(\mu\text{-}N)Fe^{III}\}^{4+}$ product. Photolysis of **2a** (2 mM) was monitored simultaneously by UV−vis and EPR spectroscopy. The observed decrease in absorbance at 458 and 302 nm and an increase in absorbance at 346 and 386 nm is nearly complete within 40 min (Figure S7). These spectral changes are nearly identical to those observed when photolysis is performed at room temperature with the Hg-vapor lamp for 15 min (results not shown). Monitoring the reaction by EPR shows a decrease in overall spin intensity upon photolysis although a low-intensity, sharp signal near $g = 2$ also evolves. Although unreacted **2a** accounts for a majority (>90%) of the remaining spin intensity in the EPR spectrum after photolysis of **2a**, a small intensity of the signal is reasonably well modeled with the *g*-values and anisotropic line widths of the (μ-nitrido)diiron complex observed upon photolysis of *trans*-$[(cyclam)Fe(N_3)_2]^+$ ($S = 1/2$; $\bar{g} =$ (2.04, 2.06, 2.20), anisotropic line widths $\bar{W} =$ (4.4, 6.9, 36.0) mT (Lorentzian)), Figure S8. A comparison of the UV−vis and EPR signal intensities collected during photolysis indicates a nearly parallel decrease of the spin intensity in the EPR (double integration values) with the loss of relative intensity in the Fe−azide charge-transfer band (458 nm) in the absorbance spectrum, Table 6. This observation is consistent with the prior Mössbauer observation which indicates the major product generated during photolysis is low-spin, $S = 0$, Fe(II).

On the basis of the observations presented above, it is concluded that in liquid solution photolysis of **2a** occurs *primarily* via homolytic cleavage of the $Fe-N_3$ bond resulting in the photoreduction of iron(III) to iron(II) and the generation of azide radical, $N_3^{\cdot}$. The photoreduction of $Fe(III)-N_3$ has previously been implicated in the formation of (μ-nitrido)diirion complexes, and Fe(II) has been directly observed in relatively small quantities upon photolysis of $Fe(III)-N_3$ complexes, but this is the first reported example of the generation of iron(II) as the major spectroscopically observable product upon pho-

Table 6. Comparison of Relative EPR Spin Intensity and Electronic Absorbance Intensity at 458 nm during Photolysis of **2a** in Acetontrile[a]

time (min)	rel int EPR	rel abs 458 nm
0	1.00	1.00
10	0.63	0.60
20	0.43	0.39
30	0.39	0.34
40	0.35	0.29

[a] Photolysis was performed at −35 °C with 300 nm radiation as detailed in the Experimental Section. The EPR intensities are double integration values relative to that of an unphotolyzed portion of the reaction mixture.

tolysis of an Fe(III)−N_3 complex. Unlike previously reported Mn(III)−N_3 complexes which undergo photoreduction when photolyzed at lower wavelengths and photooxidation at higher wavelengths,[41] **2a** displays primarily photoreduction at wavelengths as high as 300 nm in liquid solution. Attempted photolysis of a 20 mM solution of **2a** at 419 nm resulted in no detectable changes in the Mössbauer spectrum after 1 h.

The stark differences in the observed products upon photolysis of **2a** versus *trans*-[(cyclam)Fe$(N_3)_2]^+$ in liquid solution is somewhat unexpected given the spectroscopic similarities of the two complexes. As noted earlier, the two complexes share nearly identical Fe(III)/Fe(II) reduction potentials, Fe−N_3 bond distances, $\nu_{as}(N_3)$ stretching frequencies, and magnetic parameters. However, the energy of the iron−azide charge-transfer band shifts from 487 nm for *trans*-[(cyclam)Fe$(N_3)_2]^+$ to 458 nm for **2a**. The main product upon photolysis of *trans*-[(cyclam)-Fe$(N_3)_2]^+$ is ultimately the mixed valent (μ-nitrido)diiron product with a $\{Fe^{IV}(\mu\text{-}N)Fe^{III}\}^{4+}$ core (80%).[23] The proposed mechanism requires formally equimolar amounts of Fe(II) and Fe(V)═N as precursors. Additionally, up to 20% Fe(II) is observed in the Mössbauer spectrum of photolyzed of *trans*-[(cyclam)Fe$(N_3)_2]^+$ indicating that photolysis proceeds via ∼60% (40% + 20%) photoreduction and ∼40% photooxidation. That is, even in the case of *trans*-[(cyclam)Fe$(N_3)_2]^+$, photoreduction is apparently favored in liquid solution. While the major product upon photolysis of **2a** is Fe(II), the Mössbauer spectrum in Figure 5 supports the presence of a minor (27% relative intensity, ∼34% of the photolyzed products) Fe(III)−Fe(IV) (μ-nitrido)diiron product which is also detectable in the EPR. Hence the ratio of photooxidation to photoreduction for **2a** is approximately 80:20 as compared to 60:40 for *trans*-[(cyclam)-Fe$(N_3)_2]^+$. Thus, the seemingly gross observed difference in detectable product between the two systems may be due to a much smaller shift in the partition between photoreduction and photooxidation.

Photolysis of 2a in Frozen Acetonitrile. Although photolysis of **2a** in liquid solution proceeds primarily via photoreduction, its photochemistry was further investigated in frozen solution. Under such conditions, *trans*-[(cyclam)Fe$(N_3)_2]^+$ yields Fe(V)═N (∼54%) and various Fe(II) (∼29%) products as determined by EPR and Mössbauer spectroscopies. Not only is Fe(V) detectable when photolysis is performed in the immobilizing frozen acetonitrile matrix, but its relative yield is slightly elevated with respect to Fe(II) as compared to liquid solution photolysis.

Samples of **2a** for photolysis at 77 K were prepared via the previously described method II.[23] Photolysis was performed on a stirred suspension of a fine snow of **2a** and acetonitrile in liquid nitrogen with 419 nm radiation in a Rayonet reactor. High conversion of the azide complex to photolyzed products was obtained after 90 min during which time the color of the snow faded from light yellow/orange to beige/white. A portion of the photolyzed snow was packed in a Mössbauer cup for analysis. A second portion was transferred at 77 K to a precooled EPR tube.

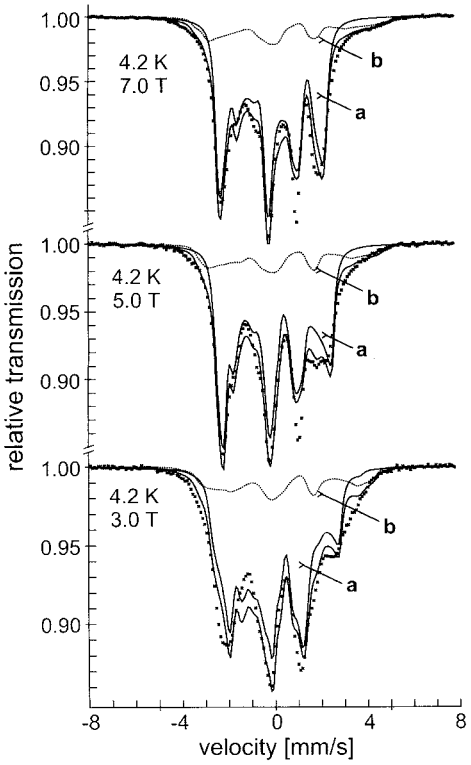

Figure 6. Magnetically perturbed Mössbauer spectra of photolyzed (77 K, 419 nm) **2a** (top, 4.2 K, 7 T; middle, 4.2 K, 5 T; bottom, 4.2 K, 3 T). The spectra were fit with two components: (a) iron(V) ($S = 3/2$) (solid line); unreacted **2a** (dashed line). Simulation parameters are given in Table 8 for iron(V) and Table 3 for **2a**. See text for discussion.

The zero-field Mössbauer spectrum of photolyzed **2a**, Figure S9, shows a high conversion of the sample (82%) to a new species with isomer shift = −0.04 mm/s and quadrupole splitting $E_Q = 1.67$ mm/s. These values are very close to those of the high-valent complex trans-[(cyclam)$(N_3)Fe^{V}$═N]$^+$ presented recently.[23] The residual part of the spectrum corresponds to remaining starting complex. Unexpectedly, formation of low-valent compound by photoreduction was not observed. One might understand this difference to the results obtained in fluid solution if the corresponding photoreduction by homolytic cleavage of azide is not effective in the frozen matrix due to recombination of Fe(II) and N_3 radicals at a faster rate in this system than bimolecular reactions of N_3 .

Magnetically perturbed measurements of the photolyzed sample confirmed the Fe(V) character of the photoproduct since they revealed the $S = 3/2$ spin state of the compound. This feature could not be obtained from EPR since at X-band frequencies resolved spectra could not be measured and sufficiently strong Q-band samples from the frozen powder material were not obtained. According to prior observations[23] it is assumed that intermolecular spin−spin interaction with traces of triplet oxygen in the low-temperature samples cause the problem. For this reason analyses of the magnetic Mössbauer spectra were restricted to those measured at fields higher than 1 T where spin−spin interactions are negligible. The field-dependent spectra, as shown in Figure 6, could be deconvoluted

(41) Meyer, K.; Bendix, J.; Metzler-Nolte N.; Weyhermüller, T.; Wieghardt, K. *J. Am. Chem. Soc.* **1998**, *120*, 7260−7270.

Table 7. Spin-Hamiltonian and Hyperfine Parameters of [(cyclam-acetato)$Fe^{V}(N)]^{+}$ and [(cyclam)$(N_3)Fe^{V}(N)]^{+}$ [23]

	[(cyclam-acetato)$Fe^{V}(N)]^{+}$	[(cyclam)$(N_3)Fe^{V}(N)]^{+}$
S	3/2	3/2
D, cm^{-1}	-0.29 ± 0.15	-0.37 ± 15
E/D	0.13 ± 0.05	0.095 ± 0.05
$\bar{g}$	2.0[a]	2.0[a]
$\bar{A}/g_{N\beta N}$, T	$(-12.8, -11.4, 1.9)$ (± 0.2)	$(-13.3, -10.6, 2.5)$ (± 0.2)
δ, mm/s	-0.04 ± 0.01[b]	-0.04 ± 0.01
ΔE_Q, mm/s[d]	-1.67 ± 0.02	-1 ± 0.02
η	0.56 ± 0.2	0.60 ± 0.2

[a] Fixed to isotropic value. [b] Taken from zero-field measurements at 80 K.

by spin-Hamiltonian simulations into the 18% contribution of nonreacted starting complex **2a** found above and the major part from high-valent iron. The appearance of the latter is quite similar to the corresponding subspectrum from *trans*-[(cyclam)-$(N_3)Fe^{V}{=}N]^{+}$.[23] Indications for the presence of low-valent species are also not observed in the magnetic Mössbauer spectra. The spin-Hamiltonian and hyperfine parameters of the high-valent $S = 3/2$ spectra of [(cyclam-acetato)$Fe^{V}{=}N]^{+}$ are summarized in Table 7, together with those of *trans*-[(cyclam)-$(N_3)Fe^{V}{=}N]^{+}$. The slight differences in zero-field splittings, A-tensors, and quadrupole splittings of both compounds are in the range expected for two metal centers with practically identical d^3 electronic structures and one differing axial ligand. The distortions from axial symmetry appear to be slightly larger for [(cyclam-acetato)$Fe^{V}{=}N]^{+}$, as can be inferred from the larger quadrupole splitting and rhombicity parameter E/D, which is plausible because of the N-functionalized cyclam core and the asymmetrically attached acetate arm.

Ozonolysis of 3. Upon exposure of a −80 °C 15 mM acetone/water (95:5) solution of **3** to a stream of ozone/oxygen, a color change from pink to intense green is observed. The green complex is stable for at least 30 min at −80 °C but decomposes quickly above −40 °C to yield an orange solution which quickly becomes turbid yielding a brown solid. No reaction is observed when oxygen is purged through the system prior to the generation of ozone. Purging of the acetone/water solution with ozone/oxygen in the absence of **3** at low temperature (−40 °C) results in a pale blue ($\lambda_{max} = 586$ nm) solution due to the dissolution of ozone.

Exposure of **3** to a stream of ozone/oxygen at −40 °C in acetone/water (95:5) results in a green species ($\lambda_{max} = 676$ nm) with a maximum intensity after 20 s. The intensity of the signal then decreases over the next several minutes, and within 6 min the intensity at 676 nm was totally attenuated. Ozonolysis reactions in dry acetone resulted in the same green species but with less intensity than the mixed-solvent system. Exposure of acetonitrile solutions of **3** to ozone at −10 °C resulted in no spectral changes other than those assigned to the dissolution of ozone.

Ozonolysis of **3** was performed at −80 °C in acetone/water (95:5) to slow the reaction and permit the collection of EPR samples over a 20 min period, Figure S10. During this time no new EPR signals are detectable while approximately 60% of the spin intensity is attenuated. Ozonolysis of **3** (35% enriched with ^{57}Fe) was performed under identical conditions for 10 min prior to freezing for Mössbauer analysis. The resulting spectrum displays one new subspectrum in addition to the starting material, Figure 7. This subspectrum is satisfactorily fit with $\delta = 0.01$ mm/s and $\Delta E_Q = 1.39$ mm/s (23% relative intensity) and is attributed to the observed green species. The negative shift in isomer shift from the iron(III) starting material is consistent with an increase in the formal oxidation state of the iron.

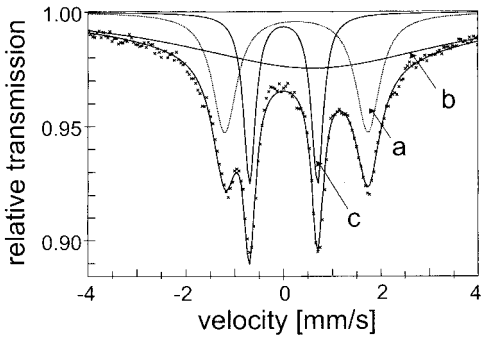

Figure 7. Zero-field Mössbauer spectrum of **3** after ozonolysis (−80 °C, 10 min) in an acetone/water mixture. The fit (solid line) is comprised of unreacted **3** (subspectra a and b) and a single, high-valent product (subspectrum c): (a) $\delta = 0.26$ mm/s, $\Delta E_Q = 2.94$ mm/s; (b) $\delta = 0.68$ mm/s, $\Delta E_Q = 0.46$ mm/s; (c) $\delta = 0.01$ mm/s, $\Delta E_Q = 1.39$ mm/s. Subspectrum b is an arbitrary fit, with a line width of >10 mm/s, of one of the components of **3** in solution, and the resulting parameters are physically meaningless. See text for further discussion.

Table 8. Relative Mössbauer Subspectral Intensities for the Ozonolysis of **3** under Various Conditions[a]

		ozonolysis	relative intensities (%)		
entry	T (°C)	time (min)	green species	decomp species	starting material
1	−80	10	21	0	79
2	−55	10	15	7	78
3	−40	0.33	23	4	73
4	−80	30	18	8	74

[a] Ozonolysis was performed on a 15 mM solution of **3** in acetone/water (95:5) as described in the Experimental Section.

Attempts were made to increase the yield of the green species by varying the temperature and duration of ozonolysis. In each case the low isomer shift subspectrum attributable to the green species is present. The only other product observable by Mössbauer spectroscopy of ozonolysis is a decomposition product obtained at higher temperatures or extended reaction times with $\delta = 0.54$ mm/s and $\Delta E_Q = 0.53$ mm/s. These parameters are consistent with high-spin iron(III) or low-spin iron(II). The results are summarized in Table 8 as the relative intensities of each of the two subspectra of the ozonolysis products with the remaining intensity assignable to starting material and not to indiscriminate decomposition of the complex by ozone. The reaction was performed at 3 temperatures. As shown in entries 1 and 2 increasing the temperature from −80 °C to −55 °C results in appearance of the decomposition subspectrum d and a decrease in the intensity of the green species, 15% versus 21%. At −40 °C, the decomposition product is observed even at short reaction times (20 s), entry 3. Increasing the ozonolysis time from 10 to 30 min, entries 1 and 4, results in an increase in the decomposition product while the amount of the green species remains constant. Under all conditions tested, the percentage of the green species is largely unchanged. The sample prepared at −40 °C was chosen for further analysis by magnetic Mössbauer spectroscopy.

Magnetic Mössbauer measurements were collected on an ozonolyzed sample (−40 °C, 20 s) and a solution of the starting material at three different external field strengths, 2, 4, and 7 T. Computer simulations of the subspectrum of the green species were used to further identify the nature of the oxidized product. The ozonolyzed sample of 3 (−40 °C, 20 s) exhibits magnetic Mössbauer spectra resembling those of the starting material;

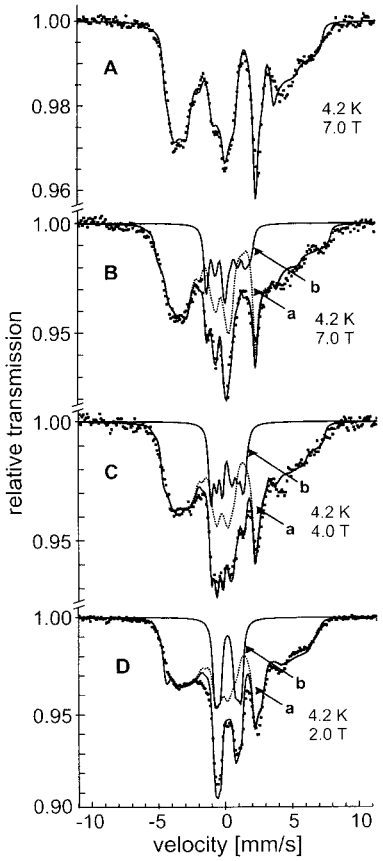

Figure 8. Magnetically perturbed Mössbauer spectra of **3** (A, 4.2 K, 7 T) and its ozonolysis product (−40 °C, 20 s) (B, 4.2 K, 7,T; C, 4.2 K, 4 T; D, 4.2 K, 2 T). The spectra of the ozonolyzed samples were fit with two components: (a) unreacted **3** (dashed line); (b) iron(IV) ($S = 1$) (solid line). Simulation parameters are given in Table 3. See text for discussion.

however, they display additional distinct lines in the center part, Figure 8. Correspondingly, the spectra could be deconvoluted into contributions of unreacted **3** and of the ozonolysis product: Subspectrum a is a simulation for the average iron-(III) material (Figure S3) with some minor variations of the respective iron(III) parameters, since the underlying two iron-(III) components of **3** were not necessarily converted with equal rates. The new species, subspectrum b, has narrow lines and weak magnetic splittings. A tentative simulation for a hypothetical $S = 0$ species (not shown) shows that the internal field is weak but not zero. The internal field is too weak to be consistent with the properties of a half-integer spin compound with $S = 1/2$ or $S = 3/2$. The corresponding $\bar{A}$-tensor components would be unrealistically low for iron(III) or iron(V) ($|A_{iso}/g_n\beta_n| < 7$ T). At the same time, a strong anisotropy is required which also would be difficult to understand. Therefore, an iron(V) species or, alternatively, an iron(IV)-radical species such as compound I of iron porphyrins[43,44] are excluded as being present in the ozonolysis product of **3**. The internal field of the species increases with the strength of the applied field. This induction effect is characteristic of integer-spin species with large ZFS and a low-lying $m_s = 0$ ground level. The resulting level mixing by moderate to strong applied fields generates sizable spin

Table 9. Spin-Hamiltonian and Hyperfine Parameters of the Ozonolysis Product of **3**, Fe(IV) ($S = 1$), and Compound II of Horseradish Peroxidase[43]

	3 + O_3	HRP II[43]
D, cm^{-1}	23 ± 2	32 ± 3
E/D	0[a]	
$\bar{g}$	2.0[b]	2.0
$\bar{A}/g_N\beta_N$, T	(−23, −23, −10) (±1)[c]	(−19.3, −19.3, −6.5)
δ, mm/s	0.01 ± 0.01[d]	0.03 ± 0.02[d]
ΔE_Q, mm/s[d]	1.37 ± 0.01	1.51 ± 0.01
η	0.80 ± 0.2	

[a] Fixed. [b] Fixed to isotropic value. [c] $A_{xx} = A_{yy}$, $A_{zz} = -10$ T fixed. [d] Taken from zero-field measurements at 80 K.

Scheme 2

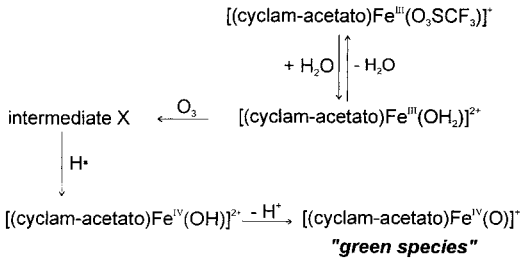

expectation values in the ground state, which leads to the observed field dependence of the magnetic hyperfine splittings. In the simulations of subspectrum b isomer shift and quadrupole splitting parameters were fixed in the simulations to the values from zero-field measurements at 80 K, the electronic g-values were fixed to 2.0, and the rhombicity parameter (E/D) was set to zero. The efg and $\bar{A}$ tensor were kept collinear to the principal axis of the of the ZFS. The $\bar{A}$ tensor was fixed axial ($A_{xx} = A_{yy}$) with the A_{zz} component arbitrarily fixed to −10 T. The three spectra (2, 4, and 7 T) were refined simultaneously with a downhill simplex procedure.[42]

Satisfactory fits are obtained for monomeric, low-spin ($S = 1$) iron(IV). The high-spin ($S = 2$) alternative is considered less likely but cannot be excluded on the basis of the magnetic Mössbauer measurements. The fit of the field dependence requires a large, positive ZFS parameter D (23 cm^{-1}) with a small rhombicity parameter E/D (0, fixed). The final fit parameters are summarized in Table 9. Attempts to fit the spectra with a dimer model require unusually small coupling constants ($J = -7 \pm 2$ cm^{-1}) for ZFS parameter D between −30 and + 30 cm^{-1} and unacceptably high D values (600 cm^{-1}) when J is fixed to a value more consistent with an oxo-bridged dimer, −100 cm^{-1}.

The EPR and Mössbauer data described above indicate clearly that the green species obtained upon ozonolysis of **3** is a monomeric, iron(IV) complex; most likely with $S = 1$. It is proposed that this species is an (oxo)iron(IV) species generated as detailed in Scheme 2. Displacement of triflate by solvent precedes reaction of **3** with ozone, which oxidizes the iron center

(42) Press: W. H.; Flannery, B. P.; Teukolsky, S. A.; Vettering, W. T. *Numerical Recipes*; Cambridge University Press: Cambridge, U.K., 1990.

(43) (a) Moss, T.; Ehrenberg, A.; Bearden, A. J. *Biochemistry*, **1969**, *8*, 4159−4162. (b) Schulz, C. E.; Rutter, R.; Sage, J. T.; Debrunner, P. G.; Hager, L. P. *Biochemistry*, **1984**, *23*, 4743−4754.

(44) (a) Boso, B.; Lang, G.; McMurry, T. J.; Groves, J. T. J. Chem. Phys. **1983**, *108*, 507−508. (b) Mandon, D.; Weiss, R.; Jayaraj, K.; Gold, A.; Terner, J.; Bill, E.; Trautwein, A. X. *Inorg. Chem.* **1992**, *31*, 4404−4409 and references therein. (c) Jayaraj, K.; Gold, A.; Austin, R. N.; Ball, L. M.; Terner, J.; Mandon, D.; Weiss, R.; Fischer, J.; DeCian, A.; Bill, E.; Müther, M.; Schünemann, V.; Trautwein, A. X. *Inorg. Chem.* **1997**, *36*, 4555−4566. (d) Jayaraj, K.; Gold, A.; Austin, R. N.; Mandon, D.; Weiss, R.; Terner, J.; Bill, E.; Müther, M.; Trautwein, A. X. *J. Am. Chem. Soc.* **1995**, *117*, 9079−9080 and references therein. (e) Wolter, T.; Wolfram, M.-K.; Müther, M.; Mandon, D.; Winkler, H.; Trautwein, A. X.; Weiss, R. *J. Inorg. Biochem.* **2000**, *78*, 117−122.

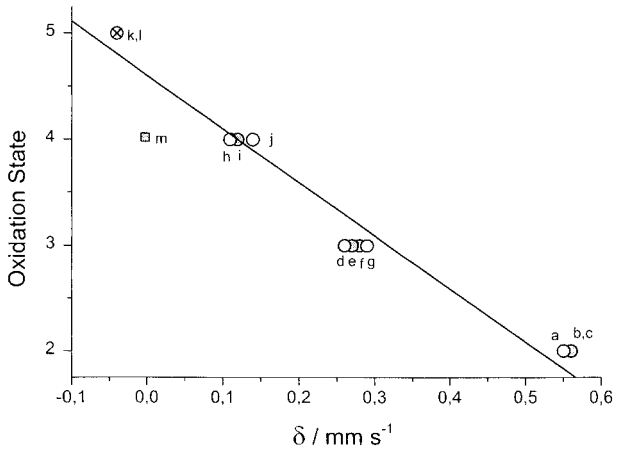

Figure 9. Plot of the isomer shift, δ, versus the formal oxidation state of iron for planar cyclam complexes: (a) *trans*-[(cyclam)$Fe^{II}(N_3)_2$]; (b) [(cyclam-acetato)$Fe^{II}(N_3)$]; (c) [(cyclam-acetato)$Fe^{II}Cl$]; (d) [(cyclam-acetato)$Fe^{III}(O_3SCF_3)]^+$; (e) [(cyclam-acetato)$Fe^{III}(N_3)]^+$; (f) [(cyclam-acetato)$Fe^{III}Cl]^+$; (g) *trans*-[(cyclam)$Fe^{III}(N_3)_2$]; (h) [(cyclam)(N_3)-Fe^{III}=N=Fe^{IV}(cyclam)$(N_3)]^{2+}$, S = 1/2; (i) [(cyclam-acetato)-Fe^{III}=N=Fe^{IV}(cyclam-acetato)$]^{2+}$, S = 1/2; (j) [(cyclam)(N_3)-Fe^{III}=N=Fe^{IV}(cyclam)$(N_3)]^{2+}$, S = 3/2; (k) [(cyclam-acetato)Fe^{V}=N$]^+$; (l) *trans*-[(cyclam)$Fe^{V}(N_3)$(N)$]^+$; (m) [(cyclam-acetato)Fe^{IV}=O$]^+$. Filled circles represent data from the current investigation, while open circles are for complexes from ref 23. The ⊗ represents 2 points, one from the current report and one from ref 23. Point m represents [(cyclam-acetato)Fe(O)$]^+$, which was not included in the linear regression calculation. The line is the result of a least-squared fit of 12 points and is defined as follows: oxidation state = 4.6(1) − 5.0(3) × (isomer shift) with R^2 = 0.98.

generating X which is either an (oxo)iron(V) or (ozonido)iron-(IV) complex. The highly oxidizing intermediate X then abstracts a hydrogen atom to yield (hydroxo)iron(IV). Deprotonation of the (hydroxo)iron(IV) complex would then yield the proposed (oxo)iron(IV) species. Attempts to transfer an oxygen atom to cyclohexene were complicated by excess ozone in the reaction mixture, but no cyclohexene oxide was observed.

The assignment of the high-valent species as an (oxo)iron-(IV) is corroborated by the strong similarities of the spin-Hamiltonian and hyperfine parameters with those of compound II of horseradish peroxidase (HRP).[43] Upon reaction of the heme iron protein HRP with excess hydrogen peroxide the (oxo)iron-(IV) cation radical, compound I, is obtained. Compound I undergoes a one-electron ligand-based reduction to yield compound II. Both compound II and the ozonolysis product of **3** display magnetic Mössbauer spectra consistent with a low-spin (S = 1) monomeric Fe(IV) ion. Additionally, Que and co-workers recently reported a dinuclear Fe(III)/Fe(IV) complex containing a terminal (oxo)iron(IV) moiety upon oxidation of a bis(μ-oxo)diiron(III) complex.[45]

The Mössbauer isomer shifts of the (cyclam-acetato)iron complexes can be correlated with their known or postulated oxidation states. Figure 9 shows this almost linear diagram which includes also the values for the corresponding complexes of nonfunctionalized (cyclam)iron complexes presented previously.[23] Such correlations which have been used before[30,46−48] are justified by the linear dependence of isomer shifts on the charge density at the ^{57}Fe Mössbauer nucleus.[30] For the

Scheme 3

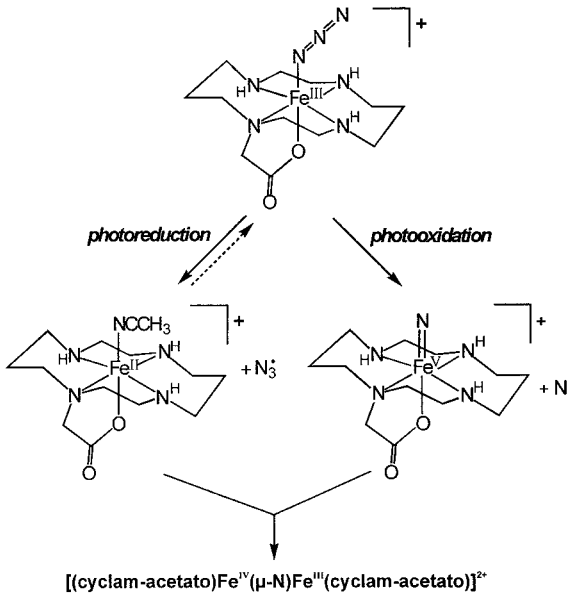

consistency of experimental diagrams with respect to formal oxidation states it is critical that the variations in the coordination sphere of the iron complexes are kept to a minimum and that the changes in the electron configurations are restricted to either the subspace of t_{2g} or of e_g orbitals. In our series all members have the "rigid" cyclam equatorial ligands and only minor changes in the axial positions. The "fifth" ligand is always acetate for the cyclam-acetate complexes and azide for the *trans*-cyclam complexes, whereas the "sixth" ligand changes for both series from N_3^- for Fe(II) and Fe(III) states to a bridging nitrido groups in the oxidation state IV (dinuclear *trans*-cyclam complexes only) to the terminal nitrido ligand for Fe(V). The variations of the electron configuration in the series occur only in the t_{2g} orbitals. The close correlation found in the diagram strongly supports the proposed assignments of oxidation states and additionally shows that these "formal" oxidation states in fact can be reasonably described by $3d(t_{2g})^n(e_g)^0$ electron configurations of iron. The only "runaway" in our diagram is the oxo complex from ozonolysis for which we postulated an Fe(IV)=O core. Its isomer shift would correlate much better with those of the (nitrido)iron(V) complexes. However, the integer spin state clearly contradicts such a tempting reassignment. It appears that the electronic structure of the high-valent compounds is rather dominated by the properties of the nitrido or oxo ligand and those are obviously different.

Conclusions and Comments. The successful spectroscopic identification of (nitrido)iron(V) in very high conversion has been accomplished through the combination of a redox innocent ligand and the use of an immobilizing matrix. The importance of the immobilizing matrix is evidenced by the dependence of product distribution on the supporting matrix. In liquid solution at temperatures as low as −35 °C, (nitrido)iron(V) is not directly observed and instead its existence is only inferred from the presence of a small amount of a (μ-nitrido)diiron product. Quite interestingly, for **2a** in liquid solution the primary photoproduct is Fe(II) resulting from heterolytic cleavage of the $Fe-N_{azide}$ bond (photoreduction). The dinuclear [Fe(μ-N)Fe]$^{4+}$ species is proposed on the basis of the similarities in the Mössbauer and

(45) Zheng, H.; Yoo, S. J.; Münck, E.; Que, L., Jr. *J. Am. Chem. Soc.* **2000**, *122*, 3789−3790.
(46) Greenwood, N. N.; Gibb, T. C. *Mössbauer Spectroscopy*; Chapman and Hall Ltd.: London, 1971.
(47) Guenzburger, D.; Esquivel, D. M. S.; Danon, J. *Phys. Rev. B* **1978**, *18*, 4561.
(48) Russo, U.; Long, G. J. Mössbauer Spectroscopic Studies of the High Oxidation States of Iron. In *Mössbauer Spectroscopy Applied to Inorganic Chemistry*; Russo, U., Long, G. J., Eds.; Plenum Press: New York, London, 1989; Vol. 3, p 289.

EPR spectra to the photolysis product of *trans*-[(cyclam)Fe-$(N_3)_2]^+$, Scheme 3. These observations are consistent with photolysis proceeding partially (∼20%) via photooxidation but primarily (∼80%) via photoreduction. However, in frozen acetonitrile a single product with Mössbauer parameters consistent with Fe(V) ($S = 3/2$) is observed. Thus, a shift from primarily photoreduction in liquid solution to primarily photooxidation in frozen solution has occurred. Likely, the reduced mobility of the azide radical in frozen solution makes the photoreduction pathway partially reversible, thus increasing the observable yield of the photooxidation pathway.

Attempts to generate (oxo)iron(V) via oxidation of **3** with ozone at −78 °C in acetone/water resulted, instead, in the detection of an (oxo)iron(IV) species. That (oxo)iron(V) eludes detection under these conditions is not unexpected given the necessity of an immobilizing matrix to provide stability for the presumably less sensitive corresponding (nitrido)iron(V) derivative. It is impressive nonetheless that ozonolysis provides a single, assignable product and not merely indiscriminate destruction of the metal complex. It is proposed, that, if generated, the (oxo)iron(V) intermediate is highly oxidizing and quickly abstracts a hydrogen atom from the nearest available source followed by deprotonation yielding the proposed (oxo)iron(IV) product. The green species detected upon ozonolysis displays spin-Hamiltonian and hyperfine parameters similar to compound II of horseradish peroxidase.

Acknowledgment. C.A.G. thanks the Alexander von Humboldt Foundation for a postdoctoral fellowship.

Supporting Information Available: Tables of crystallographic and structural refinement data, atom coordinates and U_{eq} values, bond lengths and angles, anisotropic thermal parameters, and calculated and refined positional parameters of hydrogen atoms for complex **2b** and noncrystallographic data including magnetic Mössbauer spectra of **2a** and **3**, cyclic voltammograms of **1** and **2a**, UV−vis and EPR spectra of photolyzed **2a**, zero external field Mössbauer of photolyzed (300 nm, 77 K) **2a**, and EPR of **3** recorded during ozonolysis. This material is available free of charge via the Internet at http://pubs.acs.org.

IC0005238